Radially polarized and passively Q-switched Nd:YAG laser with composite structure of gain medium

Kegui Xia (夏克贵) and Jianlang Li (李建郎)*

Shanghai Institute of Optics and Fine Mechanics, Chinese Academy of Sciences, Shanghai 201800, China

**Corresponding author: apuli@siom.ac.cn*

Received March 2, 2011; accepted April 28, 2011; posted online August 3, 2011

We report on a radially polarized and passively Q-switched Nd:YAG/Cr^{4+}:YAG laser. The bulk Nd:YAG crystal is bonded with two undoped YAG crystal end caps to weaken the thermal lens effect and thus, enhance the extraction of stored energy in the bulk gain material. In the absence of active water cooling, the average laser power reaches 383 mW with 33% slope efficiency, and the laser pulse achieves 1.457-W peak power, 18.9-ns duration, and 13.9-kHz repetition rate with 97.6% polarization purity.

OCIS codes: 140.3460, 140.3538, 140.3540, 140.3480.

doi: 10.3788/COL201109.101402.

The radially polarized laser beam shows axial symmetry both in amplitude and polarization[1−3]. The beam is applied in a variety of fields[3−8], such as particle trapping and acceleration[5], high-resolution microscopy[6], and material processing (e.g., metal cutting or drilling). Because radially polarized light is globally of the p-type with respect to the cutting surface, the material absorption to the irradiation could be maximized, the significant effect of the cutting depth and cutting speed can be facilitated[7,8]. This advantage has created a high demand for high power and radially polarized lasers.

Generally, high-power and radially polarized light are generated by combining the radial-polarization control with Q switching. This allows the production of pulsed laser beam with a high peak power and a short duration inside one laser resonator. Previously Pohl reported the generation of a radially polarized pulse from a ruby laser, in which an organic dye was used as the saturable absorber with a calcite-based telescope structure as polarization mode selector[9]. However, this method encountered difficulty in keeping stability owing to the complicated and mode-sensitive cavity configuration, as well as the poor durability of dye Q-switch.

Li *et al.* reported a radially polarized and passively Q-switched excitation of a laser-diode end-pumped Nd:YAG microchip laser[10]. They utilized a multilayer concentric sub-wavelength grating mirror as the polarization selector and a Cr^{4+}:YAG absorber as the passive Q switch. The compact configuration of this end-pumped microchip, combined with the Q-switching technique, provided high laser efficiency and excellent modal symmetry control, as well as a high peak power and nanosecond pulse. However, with the shift to higher pumping, the output power of the laser dropped significantly. Consequently, thermal lensing effect was observed in the end-pumped and millimeter-thick gain microchip in the presence of active water cooling. It should be noted that without active cooling, the laser could not oscillate. At present, the thermal problem is believed to be an obstacle for the end-pump microchip laser to reach kilowatts-peak-power laser pulse.

In this letter, we demonstrate a nature-cooled, Q-switched, and radially polarized Nd:YAG/Cr^{4+}:YAG laser, in which the Nd:YAG crystal is bonded by two undoped YAG end caps, and the high thermal conductivity of the composite structure of the gain medium is used to weaken the temperature gradient in the lasing area. We obtained a radially polarized laser pulse with high peak power without the limitation of the thermal lens effect on power scaling.

Figure 1 shows the diffusion-bonded Nd:YAG crystal used as the gain medium. It consists of a 2-mm-thick and 1 at.-% Nd:YAG and two 3-mm-thick and undoped YAG end caps combined by optical contact method and further bonded under high temperature. The front surface of the bonded crystal was coated for high transmission at 808 and 1 064 nm, and the rear surface was antireflection-coated at 1 064 nm. The whole crystal is surrounded with copper plates, except for two 2-mm diameter tunnels drilled along the cavity axis. The pumping light from a fiber-coupled 808-nm laser diode was focused into the Nd:YAG crystal. The plane mirror M1 was coated for high transmission at 808 nm and total reflection at 1 064 nm and used as the front mirror of the laser cavity; the distance between M1 and the front surface of the bonded crystal was 13.5 mm. A piece of Cr^{4+}:YAG crystal was used as the saturable absorber with antireflection coating at both surfaces and an initial transmission of 95% at 1 064 nm. We used a photonic crystal grating as the output coupler, composed of alternating high- and low-refractive-index (Nb_2O_5/SiO_2) layers, with each layer shaped into triangular and concentric corrugations. The form-birefringence effect of such subwavelength grating

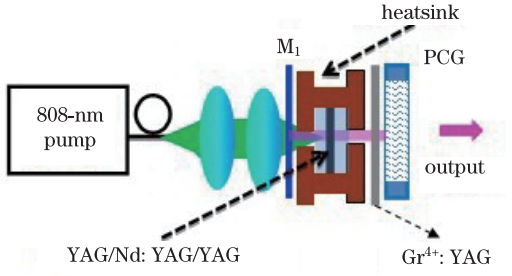

Fig. 1. Experimental setup of the LD end-pumped and bonded Nd:YAG laser.

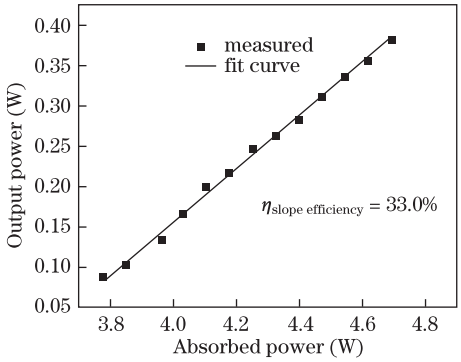

Fig. 2. Laser power as a function of absorbed pump power.

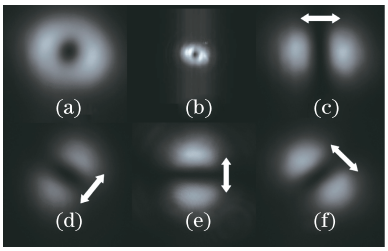

Fig. 3. (a) Far-field intensity and (b) near-field intensity distributions of the full beam profile; (c)–(f) variations of far-field intensity distributions of the passage beam through the polarizer analyzer with different orientations of the polarizer axes (white arrows indicate the directions of the axis of the polarizer analyzer).

and the resonant interference of its multilayer structure cause polarization-dependent bandpass characteristics to form[11−15]. The grating mirror used had a reflectivity of approximately 90% for transverse electric (TE) wave (radial polarization) and was transparent to transverse magnetic (TM) wave (tangential polarization) at 1 064 nm. The total length of the laser cavity was 40 mm. The laser power and beam profile were monitored by a power meter and charge-coupled device (CCD) camera, respectively. The temporal behavior of the output was recorded by a digital oscilloscope with a fast InGaAs photodiode.

When the center of the grating was positioned at the cavity axis, the laser emitted Q-switched pulses with an annular beam profile above the lasing threshold. Figure 2 plots the function relations between the laser output powers and absorbed pump power (P_{abs}). The threshold pump power, labeled as P_{abs}, was 3.53 W. When the pump power was elevated further, the laser powers increased linearly with slope efficiencies of 33% and reached 383 mW at $P_{\text{abs}} = 4.68$ W. The laser output powers could be scaled further with a higher pump power, if available, because no saturation phenomenon occurred.

The far- and near-field full profiles of the laser beams at $P_{\text{abs}} = 4.68$ W are given in Figs. 3(a) and (b), where a doughnut-shaped cross section with a central null is clearly recognizable. The state of polarization was analyzed by placing a polarizer in front of the CCD camera. Figures 3(c) and (f) show the corresponding far-field intensity distributions of the passage beam at different orientations of the axis of the polarizer, where the two-lobe structure in each image is respectively parallel to the corresponding polarizer axis. It is proved that the laser output is radially polarized.

The polarization purity of the obtained laser beam was also measured based on the following principle. At every point along the ring profile of an ideal radially polarized light, the local polarization state is linearly polarized along the respective radial direction. Thus, the polarization extinction ratio (PER) could represent the whole ring laser beam. Based on this principle, a 200-μm diameter aperture was placed into the optical path at a distance of 1.5 m behind the PCG, and its position was adjusted to maximize the intensity of the transmitted light. Consequently, the PER of the transmitted light through the aperture could be measured by rotating the polarization analyzer. At $P_{\text{abs}} = 4.68$ W, we acquired a PER of 82:1, which corresponded with a polarization purity of 97.6 %.

Another characteristic of laser output is the pulsed behavior. The pulse repetition rate and pulse width (full-width at half-maximum (FWHM)) are shown in Fig. 4 as a function of the absorbed pump power. The repetition rates of the pulse increased in a nearly linear manner with the increase of pump power and reached 13.9 kHz at $P_{\text{abs}} = 4.68$ W. On the other hand, the pulse durations decreased with the increase of pump power and were shortened to 18.9 ns. Figure 5 shows the captured pulse envelope and trains by the oscilloscope at $P_{\text{abs}} = 4.68$ W, where the pulse width (FWHM) is 18.9 ns, with a repetition rate of 13.9 kHz.

Based on the average output power shown in Fig. 2, and the responding pulse repetition rate and pulse width

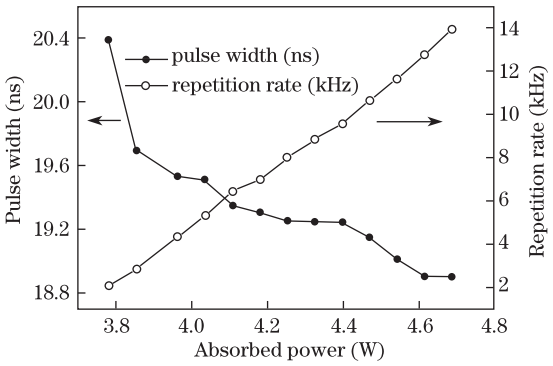

Fig. 4. Repetition rate and pulse energy as the function of absorbed pump power.

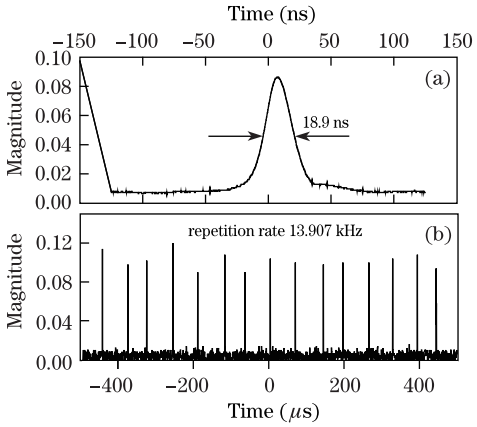

Fig. 5. Observed oscilloscope traces of (a) laser pulse train and (b) pulse envelope at $P_{\text{abs}} = 4.68$ W.

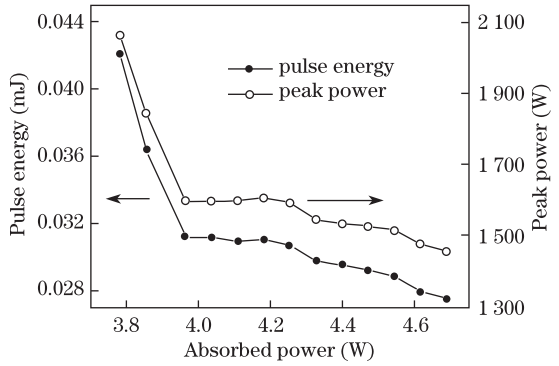

Fig. 6. Pulse energy and peak power as the function of absorbed pump power.

shown in Fig. 4, we calculate the output peak power and pulse energy of the laser. In Fig. 6, the peak power gradually decreases from 2.063 to 1.457 kW with the increase of pump power. The pulse energy decreases from 0.042 to 0.027 mJ.

In conclusion, we demonstrate a passively Q-swithed and radially polarized Nd:YAG laser. At $P_{\rm abs} = 4.68$ W, the laser pulse peak power is 1.457 kW and the FWHM is 18.9 ns, with a 13.9-kHz repetition rate and a 383-mW average power. Such radially polarized laser pulse with a high peak power and short width has considerable potential applications in metal cutting.

This work was supported by the National Natural Science Foundation of China (No. 60978025), the Hundred Talents Program of CAS, and the Shanghai Pujiang Program (No. 09PJ1410500). Kegui Xia is grateful to D. Li, Z. Fang, M. Kang, and L. Xiao for the discussion and help in the experiment. Jianlang Li acknowledges Dr. T. Sato and A. Galea from Photonic Lattice, Inc., for their support with the grating mirrors.

References

1. R. Oron, S. Blit, N. Davidson, A. A. Friesem, Z. Bomzon, and E. Hasman, Appl. Phys. Lett. **77,** 3322 (2000).
2. T. Moser, J. Balmer, D. Delbeke, P. Muys, S. Verstuyft, and R. Baets, Appl. Opt. **45,** 8517 (2006).
3. Y. Kozawa and S. Sato, Opt. Lett. **30,** 3063 (2005).
4. H. Kawauchi, K. Yonezawa, Y. Kozawa, and S. Sato, Opt. Lett. **32,** 1839 (2007).
5. A. Ashkin, IEEE J. Sel. Top. Quantum Electron. **6,** 841 (2000).
6. Q. Zhan and J. R. Leger, Appl. Opt. **41,** 4630 (2002).
7. V. G. Niziev and A. V. Nesterov, J. Phys. D **32,** 1455 (1999).
8. M. Meier, V. Romano, and T. Feurer, Appl. Phys. A **86,** 329 (2007).
9. D. Pohl, Appl. Phys. Lett. **20,** 266 (1972).
10. J. L. Li, K. I. Ueda, M. Musha, L. X. Zhong, and A. Shirakawa, Opt. Lett. **33,** 2686 (2008).
11. Y. Kozawa, S. Sato, T. Sato, Y. Inoue, Y. Ohtera, and S. Kawakami, Appl. Phys. Express **1,** 022008 (2008).
12. S. Kawakami, T. Kawashima, and T. Sato, Appl. Phys. Lett. **74,** 463 (1999).
13. A. Mehta, J. D. Brown, P. Srinivasan, R. C. Rumpf, and E. G. Johnson, Opt. Lett. **32,** 1935 (2007).
14. Y. Ohtera, T. Sato, T. Kawashima, T. Tamamura, and S. Kawakami, Electron. Lett. **35,** 1271 (1999).
15. S. Kawakami, Electron. Lett. **33,** 1260 (1997).